Received: 9 June 2017 | Revised: 20 July 2017 | Accepted: 21 July 2017

DOI: 10.1111/odi.12724

ORIGINAL ARTICLE

WILEY ORAL DISEASES

Mineral features of connective dental hard tissues in hypoplastic amelogenesis imperfecta

R Kammoun[1] | C Behets[2] | L Mansour[1] | S Ghoul-Mazgar[1]

[1]Laboratory of Histology and Embryology, Laboratory of Dento-Facial, Clinical and Biological Approach (ABCDF), Faculty of Dental Medicine, University of Monastir, Monastir, Tunisia

[2]Pôle de Morphologie, Institut de Recherche Expérimentale et Clinique, Université Catholique de Louvain, Brussels, Belgium

Correspondence
Sonia Ghoul-Mazgar, Laboratory of Histology and Embryology, Laboratory of Dento-Facial, Clinical and Biological Approach (ABCDF), Faculty of Dental Medicine, University of Monastir, Tunisia.
Email: ghoulsonia@yahoo.fr

Objective: To explore the mineral features of dentin and cementum in hypoplastic Amelogenesis imperfecta AI teeth.

Materials and methods: Forty-four (44) teeth cleaned and free of caries were used: 20 control and 24 affected by hypoplastic amelogenesis imperfecta. Thirty-two teeth were studied by pQCT, cut in sections, and analyzed under microradiography, polarized light microscopy, and confocal Raman spectroscopy. Eight teeth were observed under scanning electron microscope. Four teeth were used for an X-ray diffraction. The mineral density data were analyzed statistically with the Mann–Whitney *U* test, using GraphPad InStat software.

Results: Both coronal dentin and radicular dentin were less mineralized in AI teeth when compared to control (respectively 6.2% and 6.8%; $p < .001$). Root dentinal walls were thin and irregular, while the cellular cementum layers were thick, reaching sometimes the cervical region of the tooth. Regular dentinal tubules and sclerotic dentin areas were noticed. Partially tubular or cellular dysplastic dentin and hyper-, normo-, or hypomineralized areas were noticed in the inter-radicular areas of hypoplastic AI teeth. The main mineral component was carbonate hydroxyapatite as explored by Raman spectroscopy and X-ray diffraction.

Conclusions: Dentin and cementum in hypoplastic AI teeth are (i) hypomineralized, (ii) constituted of carbonate hydroxyapatite, and (iii) of non-homogenous structure.

KEYWORDS

amelogenesis imperfecta, dental cementum, dentin, hydroxyapatites

1 | INTRODUCTION

Amelogenesis imperfecta (AI) is a heterogeneous group of hereditary disorders that may affect the enamel of teeth (Gadhia, McDonald, Arkutu, & Malik, 2012). This disorder is classified into four main groups, depending on the clinical presentation of the defects and the stage of enamel formation that is primarily affected (Aldred, Savarirayan, & Crawford, 2003). These groups are identified as (i) hypoplastic, (ii) hypocalcified/hypomineralized, (iii) hypomature, and (iv) hypomineralized/hypomature AI with taurodontism. For the hypoplastic type, pathological processes of mineralization, called calcinosis, are particularly described in the connective tissues of AI patients. Such calcinosis could be described in either kidneys, gingivae, or dental pulp (de la Dure-Molla et al., 2014). The complex process by which precipitations of inorganic compounds within these organic matrices occur remains unclear. Besides, little is known about the structure and the mineralized compound of the dental hard tissues of mesenchymal origin such as dentin and cementum in the context of AI and particularly for the hypoplastic type.

Dentin forms the largest portion of a tooth. It contains 70% carbonated apatite, 20% organic matrix mainly constituted by type I

Approval number 2015-Histo-001 was given by the institutional reviewing Board of the Faculty of Dental Medicine of Monastir (Tunisia) for the study in September 2015.

collagen, and 10% water by weight. The collagen matrix serves as a scaffold for crystal deposition, while the non-collagenous proteins act as inhibitors, promoters, and/or stabilizers of mineral deposition (Goldberg, Kulkarni, Young, & Boskey, 2011).

Cementum is the less mineralized tissue of the tooth (65% by weight) if compared to dentin (70%) or enamel (96%) (Berkovitz, Hollan, & Moxham, 2002). It represents a thin layer of mineralized tissue covering the root dentin and playing a critical role for the attachment of the tooth to the periodontal ligament. Two kinds of cementum are generally described: (i) the acellular cementum that is generally located on the cervical portion of the root and (ii) the cellular cementum with embedded cells called cementocytes, covering the apical portion of the root (Foster, 2012).

Whereas we know much less about the biomineralization of the cementum compared to the dentin, it is admitted that mineral component of these dental mineralized connective tissues consists of biological apatite $Ca_{10}(PO_4)_6(OH)_2$ producing crystals when repeated. Any ion substitution in the apatite generates variation in the properties of the hard tissue. The presence of carbonates, for example, increases the susceptibility of hydroxyapatite (HA) to acid attack and solubility.

Considering that (i) different altered processes of mineralization are described in several connective tissues of AI patients and (ii) the tooth development is controlled by mutual interactions between an epithelium and the underlying mesenchyme, the hypothesis of this study was that not only the enamel, but also the dental hard tissues of mesenchymal origin are affected in AI teeth.

The aim of this study was to explore the dentin and the cementum in hypoplastic type of AI teeth exploring their mineral, their structure, and their ultrastructure features.

2 | MATERIALS AND METHODS

The study was performed in accordance with the Declaration of Helsinki, and an informed consent was obtained from the patients or their parents.

2.1 | Sample collection

A total of 44 teeth were used in this study. Twenty-four of them, including 4 primary and 20 permanent teeth extracted for prosthetic reasons, were collected from eight patients (18–25 years old) diagnosed with an autosomal recessive amelogenesis imperfecta of hypoplastic type. Twenty other teeth, free of caries or structural abnormalities, including 4 primary and 16 permanent teeth, extracted for orthodontic reasons, were collected from 12 healthy control patients (9–30 years old). No impacted tooth was included in this study.

All the teeth were fixed in 10% formalin during 10 days and then rinsed and cleaned. Among the 44 teeth, 32 were first used for pQCT. Then, these teeth were cut in longitudinal sections and analyzed by microradiography, polarized light microscopy, and confocal Raman spectroscopy. Eight other teeth were used for observations under scanning electron microscope, and the last four teeth were used for an X-ray diffraction.

2.2 | Peripheral quantitative computed tomography (pQCT)

Quantitative approach of pQCT interested 32 teeth (16 with AI and 16 controls).

The teeth were removed from the fixative liquid and scanned with a pQCT Research SA+ (Stratec, Pforzheim, Germany) to acquire 10 longitudinal slices through each tooth (Figure 1A). The slice thickness of 150 μm and the voxel size of 0.070 × 0.070 mm lead to a slow translation of the X-ray source (1 mm/sec) (Cornelis, Mahy, Devogelaer, De Clerck, & Nyssen-Behets, 2010). Slices were analyzed with the built-in XCT 5.4 software of the pQCT. Ten square regions of interest (ROIs) of about 0.250 mm^2 were defined in each slice: five ROIs in coronal dentin and five ROIs in radicular dentin. Consequently, for each tooth 100 equal ROIs were determined in dentin. The mean bone mineral density (BMD), proportional to the attenuation of the X-ray beam within the corresponding voxels, was measured for each ROI and expressed as $mgHA/cm^3$. The density of dentin, assumed to be similar to cortical bone, was calculated with the same thresholds: 280 mg/cm^3 (air *vs* mineralized tissue) and 400 mg/cm^3 (trabecular *vs* cortical bone). The values of the analyzed slices were averaged for each type of dentin.

2.3 | Microradiography

Thirty-two teeth were dehydrated and embedded in methylmethacrylate without preliminary decalcification. After polymerization, they were cut with a diamond saw (Leitz, Wetzlar, Germany) into 300-μm-thick sections. The sections were reduced to a uniform thickness of 100 μm with a rotating grinding machine (Planapol 2; Struers, Copenhagen, Denmark) and microradiographed by placing the sections in contact with a fine grain emulsion (VRP-M, Slavich-Geola, Vilnius, Lithuania). Then, films were exposed to X radiations (Machlett X-ray tube, Baltograph BF-50/20, Balteau, Liège, Belgium) for 1 hr at 17 kV and 14 mA. X-ray films were revealed, rinsed, and fixed. The microradiographs were scanned before being mounted on histological slides.

2.4 | Polarized light microscopy

The same sections of teeth embedded in methylmethacrylate and mounted on slides were used. The observations were made with an OLYMPUS CX41RF microscope with polarized light attachments (Olympus, Tokyo, Japan) at 4 × and 20 × magnifications. Photomicrographs were taken with an Olympus digital camera E520 (Olympus, Tokyo, Japan) and analyzed with cell sense imaging software ver1.4 (Olympus, Tokyo, Japan).

2.5 | Scanning electron microscopy (SEM)

Eight teeth, six affected by AI and two control teeth, were prepared for observations under SEM. The specimens were fragmented using a coronary–apical groove as a guide fracture. Orthophosphoric acid

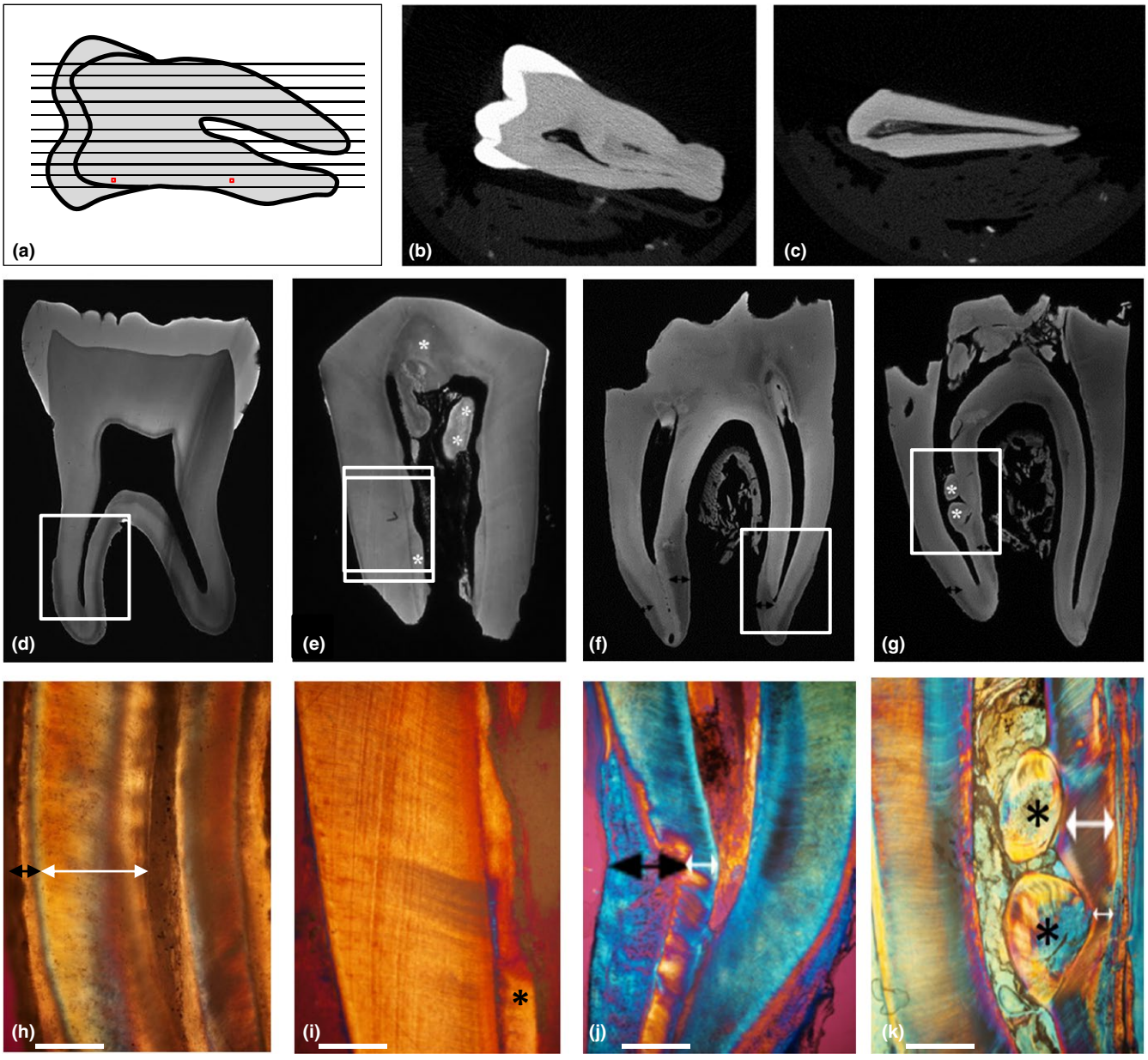

FIGURE 1 Distribution of mineralized tissues in control and Amelogenesis imperfecta (AI) teeth. (a) Schema of the scout view image showing the 10 frontal slices and the ROIs in coronal and radicular dentins as used for the mineral density measurements. (b) pQCT scan of a control tooth. (c) pQCT scan showing the reduced thickness of the enamel in a hypoplastic AI tooth. (d) Microradiograph of a control tooth. In frame, the area observed in (h) (e) Microradiograph of an AI primary tooth. Secondary dentin was observed among the root canal of the tooth and in the pulp cavity (*). Coronal pulpal calcifications were also observed (**). In frame, the area observed in (i) (f) Microradiograph of an AI permanent molar. The thickness of the dentin in the apical third of the roots is reduced, while the root morphology is conserved due to the presence of the external less mineralized tissue (black double arrows). In frame, the area observed in (j) (g) Microradiograph of an AI permanent molar. Radicular pulpal calcifications (*) were observed reducing the root canal and the thickness of the dentinal wall. The apical third of the root is composed of a thin layer of dentin covered with a thick layer of less mineralized tissue (black double arrows). In frame, the area observed in (k) (h) Healthy radicular dental tissues showing the dentin (white double arrows) and the cementum (black double arrows). (i) Secondary dentin (*) and irregular thickness of the root dentinal walls with lacunae were noticed. (j) The irregularity in the thickness of the root dentinal wall (white double arrows) is covered with a cellular cementum (black double arrows). (k) Intrapulpal calcifications (*) observed in the root canal in front of an irregular thickness of radicular dentin (white double arrows). Scale bar = 640μm [Colour figure can be viewed at wileyonlinelibrary.com]

at 37% was applied for 30 s for etching. Then, specimens were dehydrated in gradual ethanol series and were sputter-coated with gold using a JEOL (JFC-1100E) coater and then dried under vacuum and observed using high-resolution SEM (JEOL, JSM-5400).

2.6 | X-ray diffraction

Dental roots specimens for X-ray investigations were powdered by manual grinding in a mortar. The XDR patterns were recorded using X-Ray

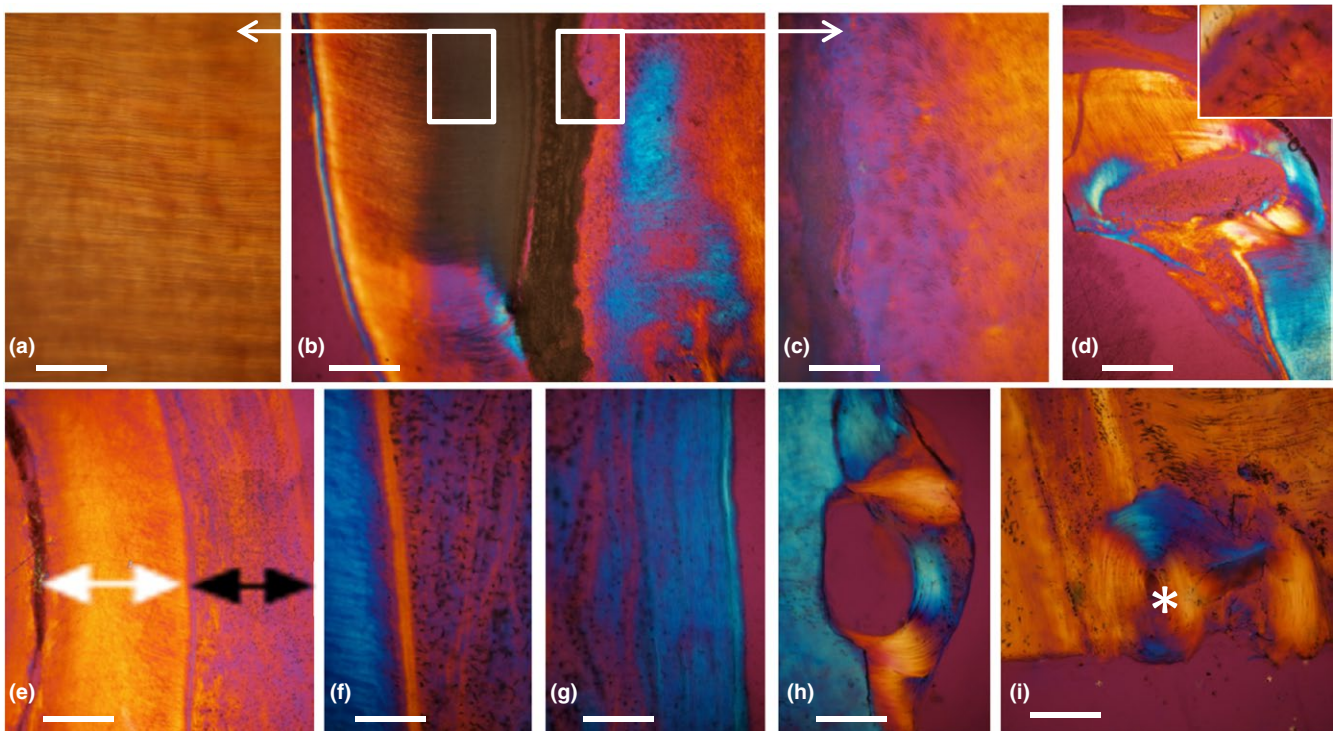

FIGURE 2 Structure of Amelogenesis imperfecta (AI) dental roots under polarized light microscopy. (a) Regular tubular dentin was observed in the external wall of the root canal (b), while the internal wall was made of irregular dysplastic dentin (c). (d) A dysplastic dentin was observed in the inter-radicular area. Higher magnification showed included cells in the dysplastic dentin. (e) The layer of the covering cellular cementum (black double arrows) was as thick as the dentin radicular wall (white double arrows). (f) A thick layer of cellular cementum was covering the root and was covered with a lamellar and cellular tissue on the surface (g). (h) Lamellar bone was noticed at the root surface of an AI primary tooth, and an osteon (*) was observed at the apical area of a resorbed root (i). Scale bar in a, c, h, and I = 160 μm, Scale bar in b, d, e, f, and g = 320 μm [Colour figure can be viewed at wileyonlinelibrary.com]

D5000 SIEMENS Diffractometer with CuKα radiation (λ = 1.54060 A°) at a power of 40 kV and 30 mA. The patterns were collected with 0.02° of step size for 2000 steps. Scan took 10 s by step for a total scan time of 33.21 min. The powder patterns were collected in the angular range of 20–60° in 2θ. The crystalline phase compositions were identified with reference to PANalytical X'pert High Score Plus 3.0.0123 software.

2.7 | Confocal Raman spectroscopy

Chemical composition analysis of radicular dentin was performed using Raman spectroscopy. Four tooth sections derived from three AI teeth and one control tooth were used for this approach. A LabRam HR 600 Raman spectrometer system equipped with a confocal microscope (Olympus) and a He–Ne laser (633 nm; HORIBA Jobin Yvon) was used to collect Raman spectra on tooth sections. Raman spectra were acquired by focusing the laser beam through a 100 × Olympus objective onto the specimens. Spectral scans were obtained over the spectral region of 50–4000 cm^{-1}.

2.8 | Statistical analysis

The mineral density mean values obtained for each tooth with the pQCT were analyzed statistically using the Mann–Whitney test. This statistical analysis was performed using GraphPad InStat software. A *p* value <.05 was considered statistically significant.

3 | RESULTS

Hypoplasia of the enamel was confirmed in the studied AI teeth as compared to control teeth, either tomographically (Figure 1b,c), radiographically (Figure 1d,e,f,g), or histologically (data not shown).

3.1 | Mineralized tissue organization in AI dental roots

In the AI affected primary teeth, despite the physiological root resorption noticed at the apical level of the root, mineralized tissue formation as secondary dentin was noticed in the inner wall of the pulp canal (Figure 1e,i). For some permanent teeth, the root dentinal walls were thin and irregular showing secondary dentin and calcifications, while the cellular cementum layers were thick and irregular (Figure 1f,g,j,k).

3.2 | Structure and ultrastructure of the dental root tissues of AI teeth

Regular dentinal tubules were observed in the AI teeth either under polarized light microscopy (Figure 2a) or with SEM (Figure 3a). Areas of dysplastic dentin were noticed by either polarized light microscopy (Figure 2b,c,d), electron microscopy (Figure 3c,d), or microradiography (Figure 4b,c,d). This dysplastic dentin was either partially tubular (Figure 2c) or cellular (Figure 2d). On the same affected teeth, sclerotic dentin was also noticed (Figure 3b).

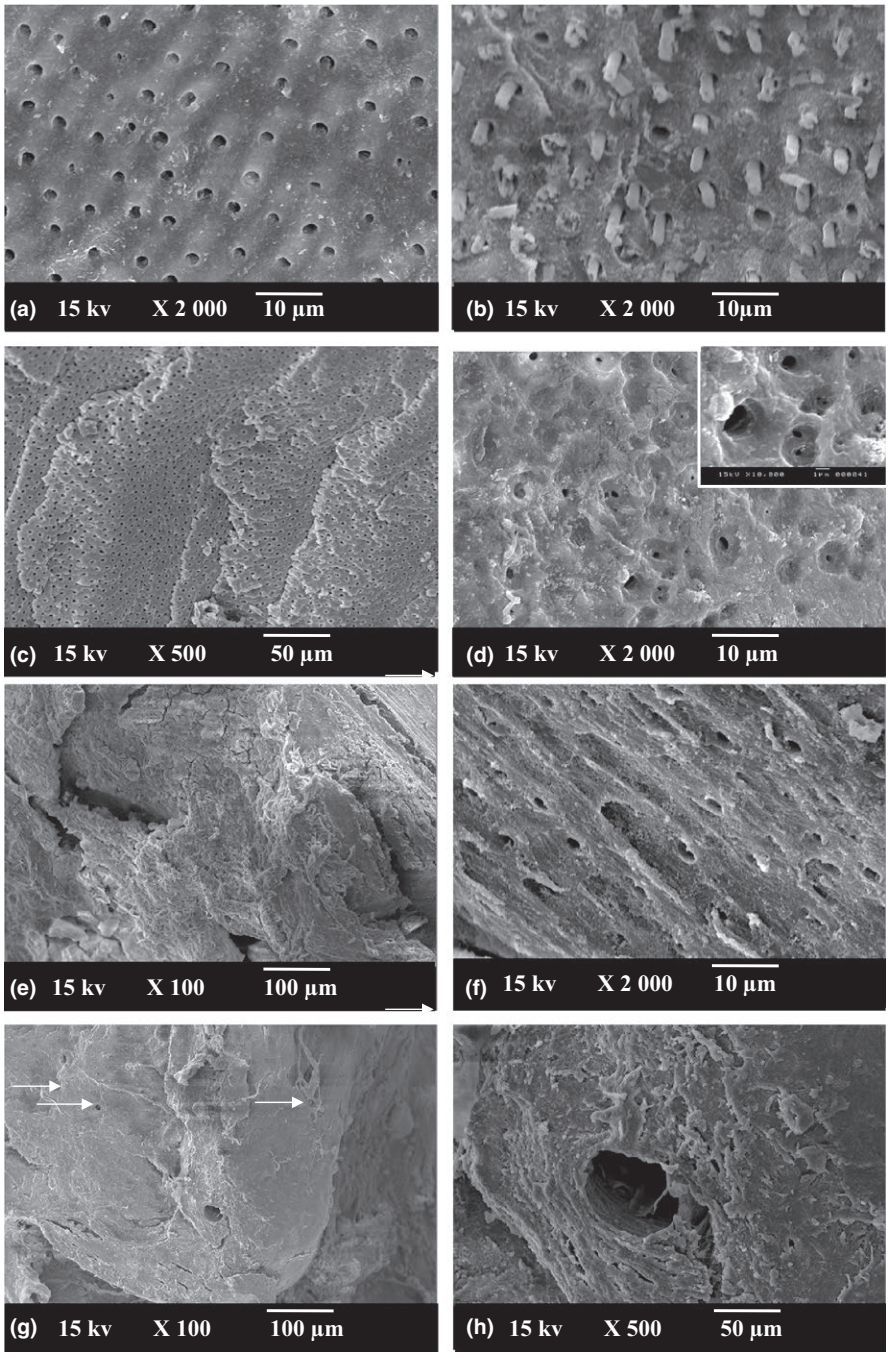

FIGURE 3 Ultrastructure of Amelogenesis imperfecta (AI) dental roots under scanning electron microscopy. (a) Regular dentinal tubules. (b) Sclerotic dentin. (c) A wave aspect of the dentin at lower magnification. (d) Cellular lacunae observed in the dysplastic dentin. Higher magnification showed several canalicules in the lacunae. (e) Fibrous cementum. (f) Cellular cementum with cementoblasts. (g) Accessory canals (arrows) in the inter-radicular dentin. (h) Higher magnification of an accessory canal

On the root surfaces, a thick layer of cellular cementum was observed (Figures 2e,f and 3e,f) that was sometimes covered itself with a lamellar tissue (Figure 2g). Particularly in primary teeth, a lamellar bone tissue was covering directly the radicular dentin without interposed cementum (Figure 2h and 2i).

3.3 | Mineral analysis of AI tissues among control and AI teeth

Analysis of the mineral density mean values obtained by pQCT (Table 1) showed that both coronal dentin and radicular dentin were less mineralized when compared to control teeth (respectively a reduced mean value equal to 6.2% and 6.8% for coronal and radicular dentins; $p < .001$). Besides, there was no significant difference between the coronal and the radicular dentin inside every studied group of teeth, neither for control teeth nor for AI teeth (Table 1; $p > .05$).

Among the AI teeth, the microradiographs of the molars revealed three different aspects of the inter-radicular dentin: either a hypermineralized (Figure 4b), a normomineralized (Figure 4c), or a hypomineralized tissue (Figure 4d) as compared to the microradiograph of a control tooth (Figure 4a). The analysis of the pQCT data among these teeth confirmed the presence of three different values of mineral density that remain significantly less mineralized when compared to the control teeth (Figure 4e).

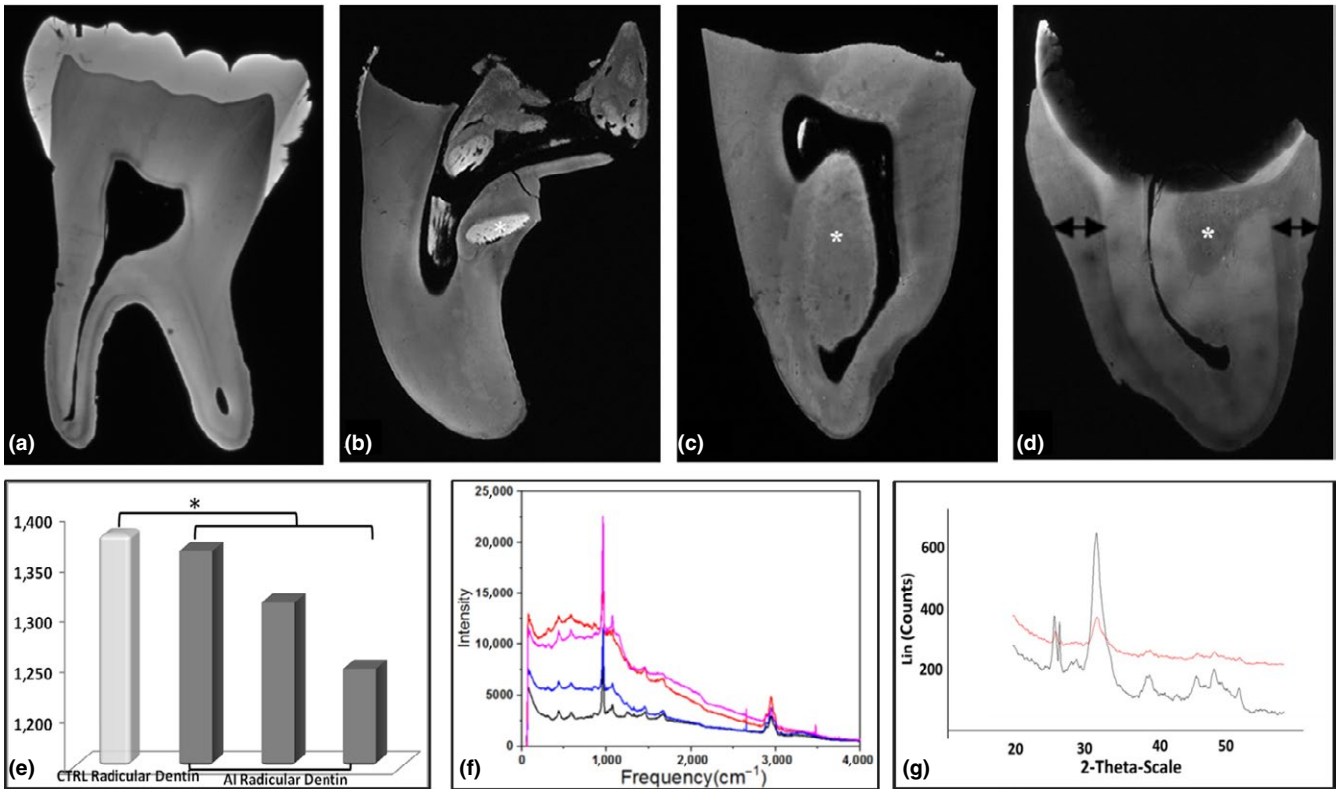

FIGURE 4 Characterization of the mineralized tissues in Amelogenesis imperfecta (AI) dental roots. Microradiograph of a control tooth (a) and AI teeth (b, c and d). (b) Hypermineralized dentin (*) was noticed in the inter-radicular area of the molar. (c) Dentin in the inter-radicular area of the molar (*) was of similar mineralization degree as circumpulpal dentin. (d) A hypomineralized tissue covering the root (black double arrows) was extending into the inter-radicular dentin (*). (e) Histogram showing means of mineral densities among control, hyper-, normo-, and hypomineralized areas in AI radicular dentin. *Statistically significant difference ($p < .001$). (f) Raman spectra comparing the control tooth and the hypo-, normo-, and hypermineralized areas noticed in the AI teeth (g) X-ray diffractograms comparing the control and the AI radicular dental hard tissues [Colour figure can be viewed at wileyonlinelibrary.com]

TABLE 1 Mineral density values of connective dental hard tissues evaluated by pQCT

	Mineral density Mean [mg/cm^3] (*SD*)			
	Control teeth	**AI teeth**	**Difference (%)**	***p***
Coronal dentin	1429 (61)	1339 (93)	6.2	<.001
Radicular dentin	1380 (44)	1285 (160)	6.8	<.001
p	>.05	>.05		

SD, standard deviation; AI, Amelogenesis imperfecta.

Raman scattering of these different areas and a control tooth revealed similar spectra. The strongest peak at 960 cm^{-1} was attributed to $V_1PO_4^{3-}$ (Figure 4f). The peaks showed that the main mineral component of the explored areas was carbonate hydroxyapatite.

X-ray diffraction patterns confirmed the hydroxyapatite nature of the permanent phases, either in AI or control teeth (Figure 4g).

4 | DISCUSSION

Amelogenesis imperfecta (AI) is a group of genetically heterogeneous hereditary conditions affecting primarily the enamel. In our study, the hypoplastic type of AI was firstly recorded according to the clinical and radiographic evaluation of each patient. Then, the hypoplastic type was also confirmed tomographically, radiographically and histologically. Our study revealed some altered features in the dental mineralized tissues of mesenchymal origin in the hypoplastic AI teeth.

Although the enamel structure and mineralization of AI teeth have been well studied in the literature using different approaches (Gopinath, Al-Salihi, Yean, Ann, & Ravichandran, 2004; Sanchez-Quevedo et al., 2001; Seymen & Kiziltan, 2002), few studies explored the structure and mineralization of dentin in these teeth. Most of these studies described an increasing mineralization (Backman et al., 1993; Belcheva, Philipov, & Tomov, 2016; Sánchez-Quevedo et al., 2004). To our knowledge, this is the first study demonstrating that dentin in AI is hypomineralized compared to control teeth. These data are opposed

to the established notions already suggested by electron microscopy. Moreover, a thickening of peritubular dentin, a partial obliteration of the dentinal tubules with a narrower lumen, and a sclerotic dentin are described in the literature (Backman et al., 1993; Sánchez-Quevedo et al., 2004), while a higher content of calcium compared to control teeth (Belcheva et al., 2016) was also mentioned. These data are interpreted by the majority of the authors as a defense mechanism of the pulp–dentin complex against external stimuli as the defective enamel cannot correctly protect the crown. We also found similar aspects of sclerotic dentin using the same approach with scanning electron microscopy. However, it should be taken into account that if this approach could give detailed information on a limited area of the dentin, these should not be generalized to all the tissue. These structural features seemed to be non-homogeneously distributed for the dentin in our study. Moreover, the higher content of calcium described in the literature in AI dentin was not associated with a higher Ca/P ratio, meaning that the detected calcium could not be completely involved in the mineralized tissue (Belcheva et al., 2016). The high level of calcium should not be considered an indicator of hypermineralization as long as it is not incorporated in a crystal. In fact, biological apatite-crystal formation in dentin is a complex process starting with heterogeneous nucleation of inorganic calcium and phosphate on an organic extracellular matrix. Organic constituents of dentine such as type I collagen provide the organizational framework for crystal deposition, whereas non-collagenous matrix macromolecules such as dentin matrix protein 1 (DMP1) are effective crystal modulators controlling mineral nucleation, transformation, and growth of hydroxyapatite (Gajjeraman, Narayanan, Hao, Qin, & George, 2007). On the other side, different mechanisms are involved in the hydroxyapatite inhibition including osteopontin and pyrophosphates. Further investigations are needed to explore the involvement of such dentin matrix components in the overall hypomineralization of dentin.

Our study also showed no significant difference in the mineralization of coronal and radicular dentins for each of the control and AI groups, when analyzed by pQCT. However, the microradiography revealed different aspects and degrees of mineralization in affected teeth. This could be attributed to the fact that our quantitative approach using pQCT was global, evaluating at least 100 values per tooth, including several dentinal areas without making the difference between the various zones. So, scanning was realized in hyper-, normo-, or hypomineralized zones, noticed in the root and inter-root areas by microradiography. Therefore, microradiography led us to further perform microscopic observations in the root and inter-root zones.

In our study, the morphologies of the roots were globally conserved. As neither the systematic reviews (de la Dure-Molla et al., 2014; Poulsen et al., 2008), nor the clinical studies (Pavlic, Battelino, TrebusakPodkrajsek, & Ovsenik, 2011), nor the AI phenotypes resulting from the mutations of concerned genes by AI (Li et al., 2016; Xie et al., 2016) have reported major abnormal root morphology, it seems that root formation in AI teeth should not be affected. However, the distribution of root tissues, dentin and cementum, among the roots appeared to be unusual. In fact, whenever the radicular dentin was thin and irregular, cellular cementum was covering this tissue sometimes reaching even the crown limits, offsetting the dentin gaps, and maintaining the root morphology. During development, Hertwig's epithelial root sheath (HERS) is usually suggested to serve as a template for root morphology (Wright, 2007). However, it is also believed that this is quite determined by the surrounding tissues. In fact, morphologically the HERS is located between the inside growing dental papilla and the outside surrounding dental follicle, and it is believed that the HERS's shape and pathway depend on the pressure and interactions exerted by these two tissues. However, mechanisms guiding tooth root shape and size remain poorly understood.

Cellular cementum was found in our study without showing features of alternation with an acellular cementum. The cellular cementum usually covers only the apical one-third of the root or appears after an injury of the root and is then called repaired cementum. Histologically, it is a bonelike mineralized tissue as it contains embedded cells in a mineralized matrix. Theoretically, cellular cementum should not function in attachment because its collagen fibers originating primarily from cementocytes run parallel to the root surface and do not protrude in the periodontal ligament space. Interestingly, cellular cementum was also observed in the cervical portion of the dental roots. Such observations were also described in the literature for transgenic mice losing the progressive ankylosis protein ANK (Foster et al., 2011). These mice showed no dental ankylosis (Nocibi et al., 2002), like the teeth described in our study. However, dental ankylosis is a frequent phenomenon in AI, suggesting that fundamental questions remain about the role of cellular cementum in protecting against the ankylosis process usually described in AI.

On the other side, when cellular cementum formation is enhanced under bisphosphonate treatment in developing rats, mineralization of root dentin and cellular cementum is prevented (Takano et al., 2003). It is thought that the released matrix components that are not sequestered in the hypomineralized dentin could also be involved in the cellular cementum development. Further investigations are needed to explore the involvement of dentinal matrix components in the development of the cellular cementum.

Our study did not only demonstrate that AI dentin is hypomineralized, but also underlined the presence of thick layers of cellular cementum close to the thin thickness of radicular dentin in some AI teeth. Although this observation was not consistent in our study, it was not rare. Such thickening of cellular cementum was also described in the literature associated with dysplastic dentin in AI molars (Nakata, Kimura, & Bixler, 1985; Peters, Cohen, & Altini, 1992; Roquebert et al., 2008). In these reports, dentin dysplasia is usually described in molar bifurcations associated with distorted and decreased root size. Such dentin dysplasia could also be involved in the abscesses and infections usually described in AI. These consistent findings indicate some localized abnormality during the formation of the bifurcation. During normal development, when the epithelial root sheath invaginates, root furcation is delineated. Deviation in this process leads to a variety of morphological root alterations such as supernumerary roots if the invaginating processes are numerous, or taurodontism if the invagination is delayed. It is worth mentioning that during root development, the Hertwig epithelial root sheath derives from the pathological enamel epithelium

of the AI teeth. Several cases of taurodontism associated with amelogenesis imperfecta are described in the literature (Dong et al., 2005; Pavlic, Lukinmaa, Nieminen, Kiukkonen, & Alaluusua, 2007), and the Dlx3 gene mutation is pointed to be associated with the autosomal dominant amelogenesis imperfecta with taurodontism (Dong et al., 2005). Interestingly, while the expression of Dlx3 during normal dental development is described in differentiated ameloblasts (Ghoul-Mazgar et al., 2005), its mutation (Choi et al., 2010) or deletion (Duverger et al., 2012) in transgenic mice is shown to be associated with major dentin defects and hypomineralization. That confirms the classical interactions described between epithelial and mesenchymal cells during tooth development and suggests that the epithelial cells would be incriminated in the appearance of the anomalies described in the dentin.

Interestingly, in our study, all our patients had an amelogenesis imperfecta of hypoplastic type with an autosomal recessive mode of transmission, suggesting that other genes than Dlx3 may be involved. In fact, several mutations of genes are described in the AI disease (de la Dure-Molla et al., 2014), and this may explain the somewhat heterogeneous results of our study. A genetic study exploring in particular the genes involved in the AI should be realized.

5 | CONCLUSIONS

This study pointed the hypomineralization of dentin in AI teeth of hypoplastic type, the carbonate hydroxyapatite nature of the mineral component, and the non-homogenous structure of the radicular dentin. While altered structures in dentin could explain the current complications of dental infections in patients with hypoplastic AI, the hypomineralization and the carbonated hydroxyapatite nature of the connective hard tissues should be taken into account during dental therapeutics involving acid-etching protocols. Further investigations are needed to explore the involvement of the released dentinal matrix components in the development of cellular cementum and the mechanisms by which the root morphology could be conserved or the dentin structure in the furcation could be affected.

ACKNOWLEDGEMENTS

The first author realized part of the experiments as visiting researcher in the “Institut de Recherche Expérimentale et Clinique” of the Université Catholique de Louvain (UCL, Belgium). Bernard Caelen, Mickaël Cardinal, and Sébastien Lafont from the UCL are thanked for their help in implementing the pQCT and microradiography approaches. Pr Zouari Ridha from the University of Sfax in Tunisia is acknowledged for his help in implementing the X-ray diffraction and Raman spectroscopy approaches.

AUTHOR CONTRIBUTION

Dr Rym Kammoun contributed to the study design, the data analysis and the writing. Dr Catherine Behets supervised the pQCT and the microradiography approaches. She also contributed writing the paper. Dr Lamia Mansour contributed to the sample collection and supervised the ethical side of the study. Dr Sonia Ghoul-Mazgar supervised the study, contributing to the study design, the data analysis, the microscopic approaches and the writing of the paper.

CONFLICT OF INTEREST

None to declare.

REFERENCES

Aldred, M. J., Savarirayan, R., & Crawford, P. J. (2003). Amelogenesis imperfecta: A classification and catalogue for the 21st century. *Oral Diseases*, *9*(1), 19–23.

Backman, B., Lundgren, T., Engstrom, E.U., Falk., L.K., Chabala, J.M., Levi-Setti, R., & Noren, J.G. (1993). The absence of correlations between a clinical classification and ultrastructural findings in amelogenesis imperfecta. *Acta Odontologica Scandinavica*, *51*, 79–89.

Belcheva, A. B., Philipov, I. A., & Tomov, G. T. (2016). Scanning electron microscopy of enamel and dentin of teeth with hypocalcified amelogenesis imperfecta. *Folia Medica*, *58*(1), 54–59.

Berkovitz, B. K. B., Hollan, G. R., & Moxham, B. J. (2002). *Oral Anatomy, histology and embryology*, 3rd ed. Mosby: Edinburgh; New York.

Choi, S. J., Song, I. S., Feng, J. Q., Gao, T., Haruyama, N., Gautam, P., … Hart, T. C. (2010). Mutant DLX 3 disrupts odontoblast polarization and dentin formation. *Developmental Biology*, *344*(2), 682–692.

Cornelis, M. A., Mahy, P., Devogelaer, J. P., De Clerck, H. J., & Nyssen-Behets, C. (2010). Does orthodontic loading influence bone mineral density around titanium miniplates? An experimental study in dogs. *Orthodontics & Craniofacial Research*, *13*(1), 21–27.

Dong, J., Amor, D., Aldred, M. J., Gu, T., Escamilla, M., & MacDougall, M. (2005). DLX3 mutation associated with autosomal dominant amelogenesis imperfecta with taurodontism. *American Journal of Medical Genetics. Part A*, *133A*(2), 138–141.

de la Dure-Molla, M., Quentric, M., Yamaguti, P. M., Acevedo, A. C., Mighell, A. J., Vikkula, M., … Bloch-Zupan, A. (2014). Pathognomonic oral profile of Enamel Renal Syndrome (ERS) caused by recessive FAM20A mutations. *Orphanet Journal of Rare Diseases*, *9*, 84. https://doi.org/10.1186/1750-1172-9-84

Duverger, O., Zah, A., Isaac, J., Sun, H. W., Bartels, A. K., Lian, J. B., Berdal, A., … Morasso, M. I. (2012). Neural crest deletion of Dlx3 leads to major dentin defects through down-regulation of Dspp. *The Journal of Biological Chemistry*, *287*(15), 12230–12240.

Foster, B. L. (2012). Methods for studying tooth root cementum by light microscopy. *International Journal of Oral Science*, *4*(3), 119–128.

Foster, B. L., Nagatomo, K. J., Bamashmous, S. O., Tompkins, K. A., Fong, H., Dunn, D., … Somerman, M. J. (2011). The progressive ankylosis protein regulates cementum apposition and extracellular matrix composition. *Cells Tissues Organs*, *194*(5), 382–405.

Gadhia, K., McDonald, S., Arkutu, N., & Malik, K. (2012). Amelogenesis imperfecta: An introduction. *British Dental Journal*, *212*(8), 377–379.

Gajjeraman, S., Narayanan, K., Hao, J., Qin, C., & George, A. (2007). Matrix macromolecules in hard tissues control the nucleation and hierarchical assembly of hydroxyapatite. *The Journal of Biological Chemistry*, *282*(2), 1193–1204.

Ghoul-Mazgar, S., Hotton, D., Lézot, F., Blin-Wakkach, C., Asselin, A., Sautier, J. M., & Berdal, A. (2005). Expression pattern of Dlx3 during cell differentiation in mineralized tissues. *Bone*, *37*(6), 799–809.

Goldberg, M., Kulkarni, A. B., Young, M., & Boskey, A. (2011). Dentin: Structure, composition and mineralization. *Frontiers in Bioscience*, *3*, 711–735.

Gopinath, V. K., Al-Salihi, K. A., Yean, C. Y., Ann, M. C., & Ravichandran, M. (2004). Amelogenesis imperfecta: enamel ultra structure and molecular studies. *The Journal of Clinical Pediatric Dentistry*, *28*(4), 319–322.

Li, L. L., Liu, P. H., Xie, X. H., Ma, S., Liu, C., Chen, L., & Qin, C. L. (2016). Loss of epithelial FAM20A in mice causes amelogenesis imperfecta, tooth eruption delay and gingival overgrowth. *International Journal of Oral Science*, *8*(2), 98–109.

Nakata, M., Kimura, O., & Bixler, D. (1985). Interradicular dentin dysplasia associated with amelogenesis imperfecta. *Oral Surgery, Oral Medicine, and Oral Pathology*, *60*(2), 182–187.

Nociti, F. H. Jr, Berry, J. E., Foster, B. L., Gurley, K. A., Kingsley, D. M., Takata, T., … Somerman, M. J. (2002). Cementum: A phosphate-sensitive tissue. *Journal of Dental Research*, *81*(12), 817–821.

Pavlic, A., Battelino, T., TrebusakPodkrajsek, K., & Ovsenik, M. (2011). Craniofacial characteristics and genotypes of amelogenesis imperfecta patients. *European Journal of Orthodontics*, *33*(3), 325–331.

Pavlic, A., Lukinmaa, P. L., Nieminen, P., Kiukkonen, A., & Alaluusua, S. (2007). Severely hypoplastic amelogenesis imperfecta with taurodontism. *International Journal of Paediatric Dentistry*, *17*(4), 259–266.

Peters, E., Cohen, M., & Altini, M. (1992). Rough hypoplastic amelogenesis imperfecta with follicular hyperplasia. *Oral Surgery, Oral Medicine, and Oral Pathology*, *74*(1), 87–92.

Poulsen, S., Gjorup, H., Haubek, D., Haukali, G., Hintze, H., Lovschall, H., & Errboe, M. (2008). Amelogenesis imperfecta- a systematic literature review of associated dental and oro-facial abnormalities and their impact on patients. *Acta Odontologica Scandinavica*, *66*(4), 193–199.

Roquebert, D., Champsaur, A., Gil de Real, P., Prasad, H., Rohrer, M. D., Pintado, M., … Koutlas, I. G. (2008). Amelogenesis imperfecta, rough hypoplastic type, dental follicular hamartomas and gingival hyperplasia: Report of a case from central America and review of the literature. *Oral Surgery, Oral Medicine, Oral Pathology, Oral Radiology, and Endodontics*, *106*, 92–98.

Sanchez-Quevedo, M. C., Ceballos, G., Garcı′a, J. M., Rodriguez, I. A., Gomez de Ferraris, M. E., & Campos, A. (2001). Scanning electron microscopy and calcification in amelogenesis imperfecta in anterior and posterior human teeth. *Histology and Histopathology*, *16*, 827–832.

Sánchez-Quevedo, M. C., Ceballos, G., García, J. M., Luna, J. D., Rodríguez, I. A., & Campos, A. (2004). Dentine structure and mineralization in hypocalcified amelogenesis imperfecta: A quantitative X-ray histochemical study. *Oral Diseases*, *10*(2), 94–98.

Seymen, F., & Kiziltan, B. (2002). Amelogenesis imperfecta: A scanning electron microscopic and histopathologic study. *The Journal of Clinical Pediatric Dentistry*, *26*, 327–335.

Takano, Y., Sakai, H., Watanabe, E., Ideguchi-Ohma, N., Jayawardena, C. K., Arai, K., … Terashima, T. (2003). Possible role of dentin matrix in region-specific deposition of cellular and acellular extrinsic fibre cementum. *Journal of Electron Microscopy*, *52*(6), 573–580.

Wright, T. (2007). The molecular control of and clinical variations in root formation. *Cells Tissues Organs*, *186*, 86–93.

Xie, X., Liu, C., Zhang, H., Jani, P. H., Lu, Y., Wang, X., … Qin, C. (2016). Abrogation of epithelial BMP2 and BMP4 causes Amelogenesis Imperfecta by reducing MMP20 and KLK4 expression. *Scientific Reports*, *6*, 25364. https://doi.org/10.1038/srep25364

How to cite this article: Kammoun R, Behets C, Mansour L, Ghoul-Mazgar S. Mineral features of connective dental hard tissues in hypoplastic amelogenesis imperfecta. *Oral Dis*. 2018;24:384–392. https://doi.org/10.1111/odi.12724